ISSN 0021-3640, JETP Letters, 2023, Vol. 117, No. 10, pp. 729–735. © The Author(s), 2023. This article is an open access publication.
Russian Text © The Author(s), 2023, published in Pis'ma v Zhurnal Eksperimental'noi i Teoreticheskoi Fiziki, 2023, Vol. 117, No. 10, pp. 727–733.

OPTICS
AND LASER PHYSICS

Diffraction-Limited Focusing of Acoustic Waves by a Mesoscopic Flat Janus Lens

O. V. Minin[a, b, *] (ORCID: 0000-0002-9749-2106), S. Zhou[c], P. F. Baranov[a], and I. V. Minin[a, b, d] (ORCID: 0000-0002-6108-8419)

[a] *National Research Tomsk Polytechnic University, Tomsk, 634050 Russia*
[b] *Siberian State University of Geosystems and Technologies, Novosibirsk, 630010 Russia*
[c] *Jiangsu Key Laboratory of Advanced Manufacturing Technology, Faculty of Mechanical and Material Engineering, Huaiyin Institute of Technology, 223003 Huai'an, People's Republic of China*
[d] *Design and Technology Institute of Applied Microelectronics, Rzhanov Institute of Semiconductor Physics, Siberian Branch, Russian Academy of Sciences, Novosibirsk, 630090 Russia*
**e-mail: prof.minin@gmail.com*

Received March 9, 2023; revised April 2, 2023; accepted April 6, 2023

Anisotropic focusing by a mesoscopic (Mie size parameter of about 18) acoustic cubic lens based on V-shaped plate structures has been simulated numerically and confirmed experimentally. It has been shown for the first time that this lens with an edge dimension of about three wavelengths ensures the focusing of an acoustic wave in air into a diffraction-limited region. In the inverse geometry of the structure, the lens completely reflects the incident acoustic wave.

DOI: 10.1134/S0021364023601045

INTRODUCTION

Sound is always present in diverse spheres of our everyday life. Acoustic lenses can be used in various fields of physics, engineering, and medicine. However, their fabrication is still a complex and relevant problem, in particular, because natural materials having properties necessary for such acoustic lenses are scarce [1, 2] since natural materials usually cannot ensure a low speed of sound and a high density simultaneously.

Various types of currently existing acoustic lenses are based on different physical phenomena: Fresnel diffraction [3, 4], two- and three-dimensional acoustic photon crystals [5–8], acoustic metamaterials [9], Helmholtz resonators [10], gradient (GRIN) structures [11], including Luneburg acoustic lenses [12], etc. However, natural acoustic materials with a gradient refractive index are absent.

Another way to obtain modern acoustic lenses is based on the use of gas-filled spherical [13–15] or mesoscopic cubic lenses with the possibility of diffraction-limited focusing [16, 17]. Acoustic lenses have the same restrictions in focusing limit as electromagnetic (optical) lenses; i.e., their resolution is limited to a half wavelength because of diffraction. Furthermore, gas-filled acoustic lenses require gases often having properties dangerous for health and the environment.

Scatterers with the Mie size parameter $q = kL = 2\pi/\lambda L$ (L is the typical outer dimension of the structure and k is the wavenumber) in the range of 5–50 have attracted particular interest recently. This range is intermediate between dipole particles ($q \ll 1$), particles with Mie resonances ($q \sim 1$, so-called Mie-tronics), and large particles ($q > 100$, including classical lenses and mirrors: the diameter of an acoustic lens at acoustic frequencies is about 2 m [18]), scattering on which can be described within geometrical optics. For this reason, scatterers with the size parameter $q \sim 10$ are sometimes called particle lenses [19]. The "acoustic jet" phenomenon [20, 21], which extends the concept of the photonic nanojet to acoustic waves and was discovered by O.V. Minin and I.V. Minin through the similarity of wave equations and Maxwell's equations for the electromagnetic waves, potentially makes it possible to obtain a subwavelength acoustic focus. We emphasize that the propagation and localization of acoustic waves through mesoscopic structures (with a characteristic size of several wavelengths) cannot be predicted within geometrical optics [19, 21, 22].

At the same time, refractive acoustic lenses, which consist of subwavelength field "modifiers," i.e., plates, rods, or disks, and form sound in the far-field region, have long been known [23]. A plate acoustic refractive lens was proposed by Kock in 1948 [24]. An artificial material of the lens was formed from an array of parallel plates placed at an angle of θ to incident radiation.

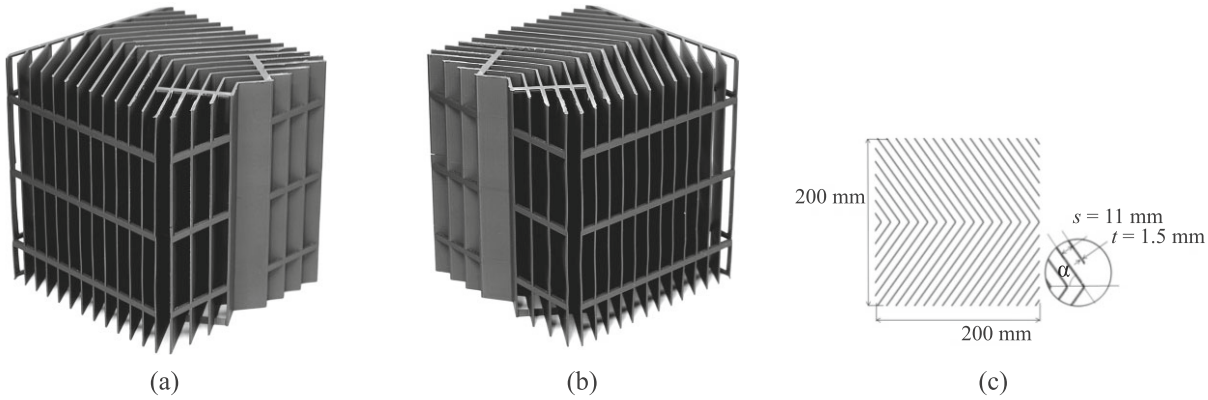

Fig. 1. (a, b) Two views of the acoustic mesoscopic Janus lens based on V-shaped plates and (c) its parameters for a frequency of 5.0 kHz.

In this system, the path covered by the acoustic wave between the inclined plates increases by a factor of $1/\cos\theta$, which corresponds to the effective refractive index $n = 1/\cos\theta$. A modification of such lenses consists of a flat plate with a nonuniform set of zigzag slits [25], whose outputs serve as secondary subwavelength sources [26].

The main aim of this work is to demonstrate the possibility of anisotropic acoustic (sound) focusing by a mesoscopic cubic Janus lens consisting of the array of V-shaped parallel plates. The term Janus lens was introduced in [27] and means in our case a kind of a mesostructure consisting of several different parts (differing in composition and/or shape) with different properties. Our simulation shows the possibility of the diffraction-limited focusing of acoustic waves in air through the lens with planar outer surfaces and the dimensions of the edges equal to three wavelengths, which is confirmed by the experiment.

MODEL AND EXPERIMENTAL SETUP

To reduce high computational and time costs required for three-dimensional simulation, the numerical simulation was performed with the finite element method implemented in the two-dimensional acoustic COMSOL Multiphysics simulation package [28]. We used a free triangular grid with the maximum dimension of an element $\lambda/8$ and the standard procedure of the adaptive compression of the grid in regions with a high pressure gradient. The incident (illuminating) plane wave was chosen for simulations. It was ensured in experiments by choosing the distance between the emitter and the lens corresponding to the far-field region.

The ABS plastic with the acoustic resistance a factor of approximately 6000 higher than that of air was used as a material for the plates of the particle lens in the calculations and experiments. Consequently, such scatterers can be considered as acoustically hard [11]. The speeds of sound C and the densities ρ used for the ABS plastic and air were $C_{abs} = 2250$ m/s, $\rho_{abs} = 1050$ kg/m^3, $C_{sabs} = 1025$ m/s, $C_{air} = 343$ m/s, and $\rho_{air} = 1.21$ kg/m^3, where C_{sabs} is the transverse velocity of sound in the ABS plastic [21, 29].

The corresponding cubic structure was fabricated using a three-dimensional printer to experimentally test the focusing properties of the considered Janus lens. The measurements were carried out in an echo-free chamber whose design and the measurement method were similar to those described in [4, 16, 17, 30, 31].

RESULTS AND DISCUSSION

The view of the Janus lens and its design features are shown in Fig. 1. It was shown in [16, 17] that it is sufficient to ensure the outer dimension of the gas-filled particle lens about three wavelengths for the efficient focusing of acoustic waves. The lens studied in this work was designed to a frequency of 5.0 kHz, the thickness of the ABS plates was $s = 1.5$ mm, the distance between the plates was $t = 11$ mm, the inclination angle of plates $\alpha = 62°$, and the edges of the cubic structure had the size $L = 200$ mm or about three wavelengths. Thus, the Mie size parameter [19, 32] of the Janus lens is $q \sim 18$; i.e., the lens is mesoscopic. The sizes of the particle lens were chosen such the particle lens can be fabricated using the three-dimensional printer and has a sufficient strength and the minimum outer size. Below, we use the geometrical parameters of the structure in units of the incident wavelength in air rather than their absolute values.

The simulated distribution of the acoustic wave intensity $I = p^2/\rho c$ divided by the parameters of the incident plane wave [31] was confirmed in experiments. They were performed with a specially developed synchronous amplifier with a differential input, and a digital processing algorithm was applied to dif-

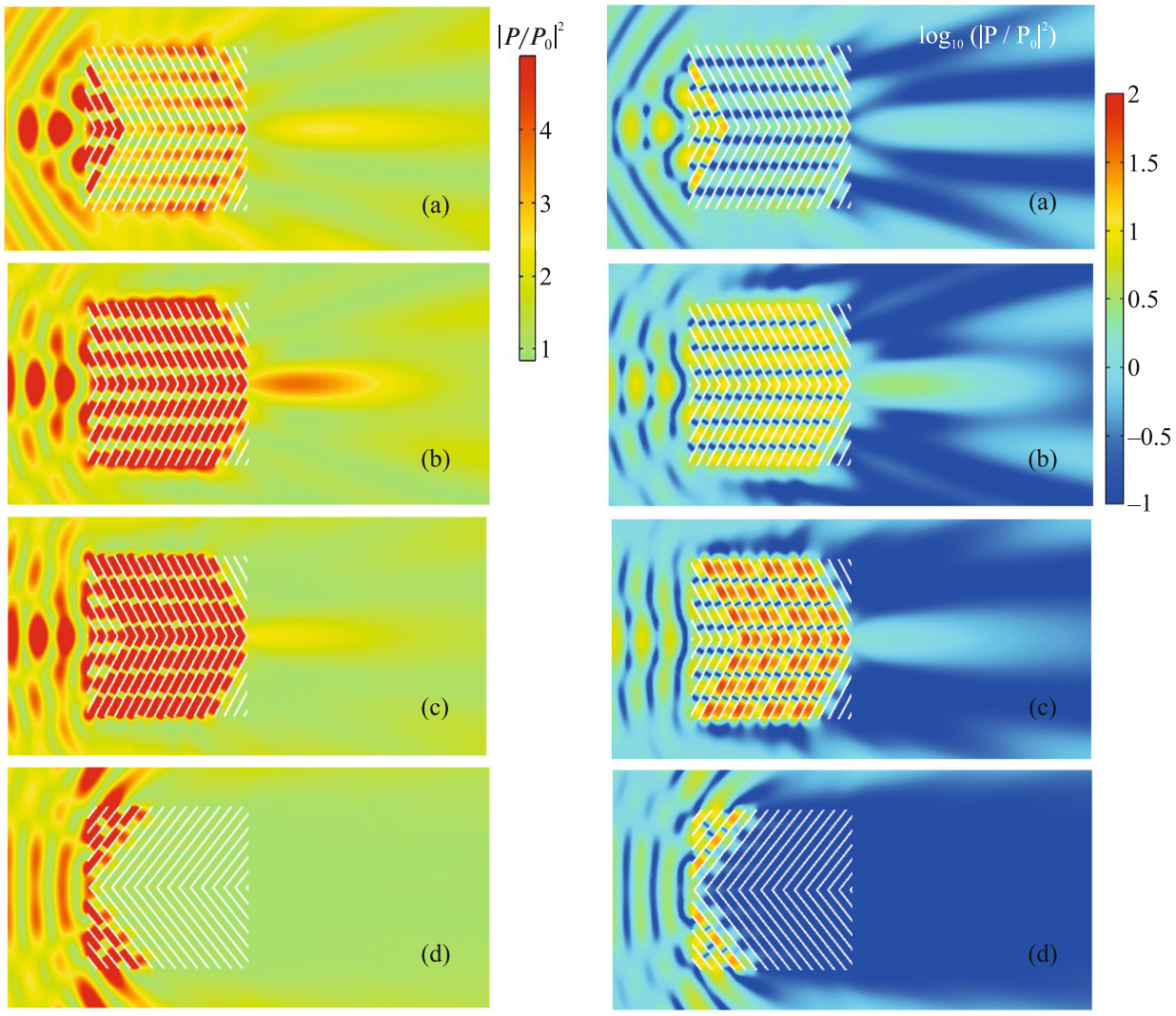

Fig. 2. (Color online) Acoustic intensity distributions divided by the parameters of the incident plane wave at frequencies of (a) 4.8, (b) 5.0, and (c) 5.2 kHz for the inclination angle of plates $\alpha = 62°$. (d) Acoustic intensity distribution for the inversion geometry of the cubic Janus lens at a frequency of 5.0 kHz. The acoustic wave propagated from the left to the right. The intensity scale in the left panels was chosen for the best visualization of the focusing region in the shadow part of the lens. The right panels present the logarithm of the same intensity distributions to demonstrate the structure of waves inside the Janus lens.

ferential signals, which reduced the uncertainty of measurements. Figure 2 presents sound intensity distributions at frequencies of 4.8, 5.0, and 5.2 kHz for the inclination angle of plates $\alpha = 62°$ obtained with the lens designed for a frequency of 5 kHz.

The presented results demonstrate that the diffraction of the incident wave occurs around the outer surface of the cubic structure. The acoustic wave is focused owing to the combination of diffraction around the structure and constructive interference with the wave transmitted through the V-shaped plate structure in the shadow part of the lens.

The frequencies of 4.8, 5.0, and 5.2 kHz correspond to the dimensions of the lens of 2.79λ, 2.92λ, and 3.03λ, respectively, where λ is the wavelength. It is clearly seen that the formation of the weak localization region of the sound field pressure begins at the dimension of the edge of the cubic lens of 2.79λ (4.8 kHz, Fig. 2a). The focusing region near the shadow surface of the lens at a cube side dimension of 2.92λ (5.0 kHz, Fig. 2b) is fully formed and has the symmetric structure of an acoustic jet [8, 16, 18]. In this case, the position of the field intensity maximum along the acoustic jet is slightly shifted to the left toward the shadow surface of the lens. With a further increase in the effective dimension of the cube to 3.03λ (5.2 kHz), the focusing effect decreases and the region of the maximum localization of the acoustic field is further shifted to the left and almost coincides with the shadow surface of the lens.

The simulation of the inversion geometry of the Janus lens (Fig. 2d) demonstrates the anisotropic properties of the focusing of the acoustic wave. In this case, the incident wave is almost fully reflected from the outer surface of the structure and the transmitted field is hardly present in the shadow region of the lens. The existence of a maximum in the shadow region of the lens at one direction of wave propagation (Fig. 2b) and the absence of any signal in the shadow region of the lens when the wave is incident on the lens from the opposite side (Fig. 2d) do not contradict the principle of reciprocity because these effects are due to the asymmetric propagation of waves at different orientations of the lens because of its structure. We note that this is not equivalent to the exchange of the source and the detector to test the principle of reciprocity. Asymmetric propagation does not mean nonreciprocity.

It is well known that the acoustic jet, which is an analog of the photon jet, is a localized narrow intense beam that can propagate at a distance exceeding the wavelength λ after leaving the shadow surface of an illuminated penetrable object with the characteristic dimension larger than the wavelength and is formed owing to the interference of the field scattered (diffracted) on the object (the particle lens) and the wave passed through it [8, 20, 33–35]. According to Figs. 2a–2c, only the channels formed by V-shaped plates in the shadow part of the particle lens contribute to the formation of the acoustic jet at different frequencies when the flow between the plates leaves in its shadow part and interferes with the field scattered on the outer surface of the particle lens (Fig. 2b). Propagating waves are converted to waves propagating along the lateral edge of the particle lens. When a wave passes through channels between the plates in the shadow part of the lens (Fig. 2b), a fraction of the acoustic wave leaves in the axial direction in its shadow part, the pressure field is redirected, and the acoustic jet is formed in the near-field region at a distance less than the wavelength from the shadow surface of the lens. In particular, if the constructive interference between the waves scattered on the cubic particle and the waves transmitted through the particle, e.g., in the case of the metallic cube with the same dimensions does not occur [8], the acoustic jet is not formed [8, 20]. The acoustic jet is stably formed in the case of a penetrable cubic particle (gas-filled, dielectric) [16, 17, 36].

The number of the "plates" (channels) located along the side edge of the lens is determined by the distance between the plates, their thickness, and the edge length of the cubic structure. As seen in Figs. 2a–2c, only plates in the shadow part of the particle lens contribute to the formation of the acoustic jet at different frequencies when the flow between the plates leaves in its shadow part and interferes with the field scattered on the outer surface of the particle lens. The particle lens completely opaque to radiation can be potentially combined with the plate structure in its shadow part. In this case, the lens was fabricated from equidistant V-shaped plates located in the entire volume of the lens for its simplicity and manufacturability.

Figure S1 in the supplementary materials shows the distribution of the relative intensity of the sound field in the considered structure for the inclination angles of plates of 60°, 61°, 63°, and 64°. The analysis of the performed simulation shows that the field localization region in the shadow part of the particle lens at the inclination angles of plates of about 60° almost coincides with its shadow surface; i.e., a peculiar "hot point" is formed. The focus (region with the maximum relative intensity along the wave propagation direction) at the inclination angle of plates of 61° (Fig. S1b) is located at about 100 mm and is shifted to about 120 mm at the inclination angle of plates of 64°.

The distribution of the relative intensity of the sound field along the side (e.g., upper in Fig. S1) edge of the particle lens is remarkable. A more uniform distribution of the field intensity along the side edge of the structure affects the formation of the field localization region (focus): as the inclination angle of plates increases from 60° to 62°–64°, the field intensity along the side edge becomes more uniform with a small increase in the amplitude toward the shadow boundary of the particle. The detailed analysis of the structure of waves and the corresponding effects inside the Janus lens is beyond the scope of this work and will be performed elsewhere.

To analyze the focusing properties of the particle lens, it is reasonable to use the time-averaged acoustic field intensity behind the particle lens $\mathbf{I} = p\mathbf{v}$ divided by the intensity of the plane wave [37, 38]. The focusing action of the particle lens is due to the acoustic field flow in channels between the plates predominantly in its shadow part. Figure S2 in the supplementary material shows the normalized intensity flow through the particle lens and near it for frequencies of the incident wave of 4.8, 4.9, and 5.1 kHz. It is seen that the wave reflected from the front surface interferes with the incident wave and forms flows along the side faces of the structure. Under the conditions of waveguide resonances in gaps between the plates (see Fig. S2b in the supplementary material), these flows constitute a flow converging to the axis, which in turn forms the focusing region (acoustic jet). The comparison of Figs. S2a and S2b in the supplementary material shows that the flow through the gap between the plates in the shadow part of the particle lens at a frequency of 4.9 kHz is more intense and, correspondingly, the focusing (field localization) region is pronounced.

At a frequency of 5.0 kHz, when the pronounced localization region of the sound field is observed in the shadow part of the lens (Fig. 2b), the flux distribution along the side edge of the lens promotes the formation of a flow between the plates along the channels of the lens in its shadow part and the escape of this flow in the axial direction. The constructive interference of

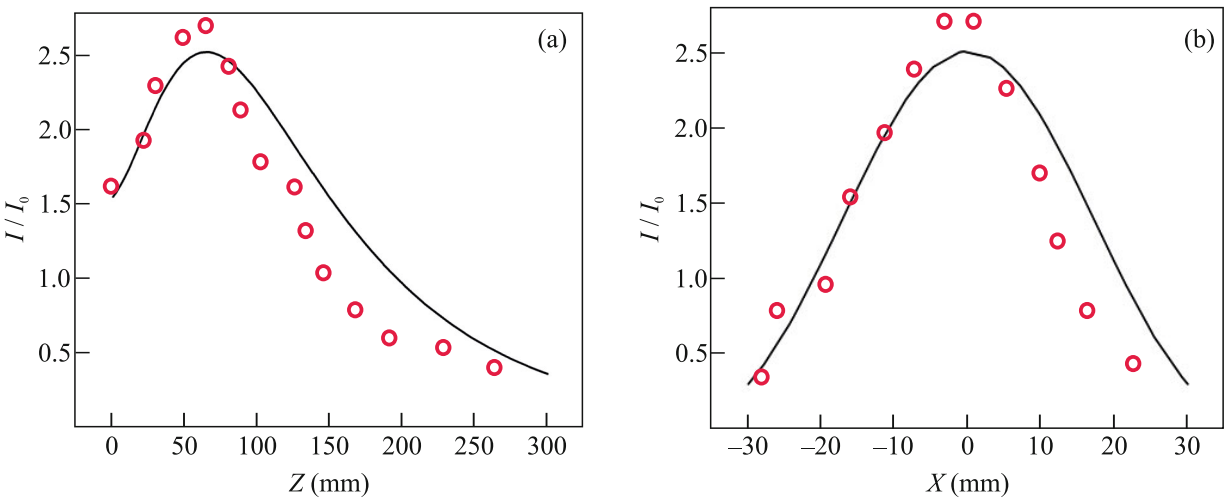

Fig. 3. (Color online) (Red circles) Experimental distribution of the relative sound field intensity (a) along and (b) across the acoustic jet in comparison with the simulation shown by the solid lines.

the field scattered by the lens with the localized axial flow in its shadow part results in the formation of the acoustic jet [8, 33, 35, 36]. This mechanism is similar to the mechanism of the formation of a photon jet in optics owing to the optimization of the tangential component of the electric field along the side faces of the cubic structure [39]. Reflection from the face surface of the particle lens and the reflection-induced structure of the energy flow along the side edges change naturally because the different effective gap and the thickness of plates depend on the frequency. According to Figs. 2 and S2b, the enhancement of the considered particle lens at a frequency of about 5.0 kHz is approximately 4 in intensity divided by the intensity of the incident wave.

Figure 3 presents the parameters of the focusing region of the acoustic wave (the characteristic of the acoustic jet) obtained in the simulation and the corresponding experiment at a frequency of 5.0 kHz. Experimental data shown Fig. 3a indicate that the length of the acoustic jet in the longitudinal direction (direction of incidence of the plane wave) is about 132 mm or 1.9λ (the two-dimensional simulation predicts a value of 2.4λ). The coordinates in Fig. 3a are measured from the shadow surface of the lens. Figure 3b characterizes the transverse dimensions of the sound field localization region (resolution) in the plane passing through the point of the maximum intensity along the acoustic jet ($Z = 65$ mm). According to this figure, the transverse dimension of the sound field localization region at a frequency of 5.0 kHz is about 31 mm or 0.45λ (the two-dimensional simulation gives 0.54λ), which is close to the diffraction limit.

The experiment yielded a somewhat higher field intensity in the acoustic jet region at smaller sizes of the corresponding distributions along and across the acoustic jet. This occurs because the simulation was performed in two dimensions [40], whereas the characteristics of the three-dimensional cubic Janus lens were measured in the experiment.

The conducted simulation showed that a superresolution of about 0.16λ can be achieved in the immediate vicinity of, e.g., the lens with $\alpha = 60°$, but the width of the distribution of the sound field intensity already at a distance of about 12 mm from the shadow surface of the lens increases to 0.43λ.

CONCLUSIONS

To summarize, a new three-dimensional mesoscopic acoustic Janus lens with flat surfaces has been proposed, designed, and fabricated on the basis of an internal two-dimensional V-shaped plate. The performed simulation and experiment are in good agreement with each other and demonstrate the diffraction-limited acoustic focusing with anisotropic properties. Focusing is three-dimensional because the cubic lens consisting of the two-dimensional V-shaped structure, similar to [8], has the three-dimensional outer shape. The enhancement of focusing intensity in water should be expected in the ultrasonic range.

An advantage of the proposed lens is that its properties are independent of the parameters of the environment because the material of the environment is included in the structure of the lens, and its relative refractive index depends only on the length of parallel plates or on the inclination angle of these plates to the direction of incident radiation. This acoustic particle lens can be applied for the subwavelength focusing of acoustic waves both in gases and in liquids. Compared to gas-filled acoustic lenses, the proposed lens has sufficient strength and reliability.

Although the method described in this work has demonstrated the possibility of the focusing of sound, e.g., for the acoustic drying of materials, control of the noise level, acoustic thermography, or new sound-focusing systems, it is also of interest for ultrasonic applications [41, 42], e.g., in biomedicine, nondestructive control, spectroscopy, acoustic levitation of particles and manipulations with them, and visualization.

ACKNOWLEDGMENTS

We are grateful to Prof. Noé Jimenez for the constructive discussion of the principle of reciprocity and the asymmetric focusing by the considered Janus lens.

FUNDING

This study was supported by the Russian Science Foundation, project no. 21-79-00083, and by the Development Program of the National Research Tomsk Polytechnic University.

CONFLICT OF INTEREST

The authors declare that they have no conflicts of interest.

OPEN ACCESS

SUPPLEMENTARY INFORMATION

The online version contains supplementary material available at https://doi.org/10.1134/S0021364023601045.

REFERENCES

1. C. Sondhauss, Ann. Phys. Chem. **85**, 378 (1852).
2. Lord Rayleigh. Proc. London Math. Soc. **S1-17**(1), 4 (1855).
3. B. Hadimioglu, E. G. Rawson, R. Lujan, M. Lim, J. C. Zesch, T. Khuri-Yakub, and C. F. Quate, in *Proceedings of the IEEE Ultrasonics Symposium, Baltimore, MD, USA* (1993), Vol. 1, p. 579. https://doi.org/10.1109/ULTSYM.1993.339544
4. D. Tarrazó-Serrano, S. Pérez-López, P. Candelas, A. Uris, and C. Rubio, Sci. Rep. **9**, 7067 (2019).
5. T. Miyashita, R. Taniguchi, and H. Sakamoto, in *Proceedings of the 5th World Congress on Ultrasonics, Paris, France* (2003), Paper No. TO-PM04.02, p. 911.
6. O. A. Kaya, A. Cicek, and B. Ulug, Acoust. Phys. **57**, 292 (2011).
7. M. Dubois, J. Perchoux, A. L. Vanel, C. Tronche, Y. Achaoui, G. Dupont, K. Bertling, A. D. Rakic, T. Antonakakis, S. Enoch, R. Abdeddaim, R. V. Craster, and S. Guenneau, Phys. Rev. B **99**, 100301(R) (2019).
8. S. Castiñeira-Ibáñez, D. Tarrazó-Serrano, P. Candelas, O. V. Minin, C. Rubio, and I. V. Minin, Results Phys. **15**, 102582 (2019).
9. Y. Li, G. Yu, B. Liang, X. Zou, G. Li, and S. Cheng, Sci. Rep. **4**, 6830 (2014).
10. X. Yang, J. Yin, G. Yu, L. Peng, and N. Wang, Appl. Phys. Lett. **107**, 193505 (2015).
11. V. Romero-Garcia, A. Cebrecos, R. Picó, V. J. Sánchez-Morcillo, L. M. Garcia-Raffi, and J. V. Sńchez-Pérez, Appl. Phys. Lett. **103**, 264106 (2013).
12. C. Lu, R. Yu, Q. Ma, K. Wang, J. Wang, and D. Wu, Appl. Phys. Lett. **118**, 144103 (2021).
13. H. Kruglak and C. C. Kruse, Am. J. Phys. **8**, 260 (1940).
14. J. M. Kendall, NASA Tech. Briefs **5**, 345 (1980).
15. D. C. Thomas, K. L. Gee, and R. S. Turley, Am. J. Phys. **77**, 197 (2009).
16. C. Rubio, D. Tarrazo-Serrano, O. V. Minin, A. Uris, and I. V. Minin, Results Phys. **12**, 1905 (2019).
17. C. Rubio, D. Tarrazio-Serrano, O. V. Minin, A. Uris, and I. V. Minin, Eur. Phys. Lett. **123**, 64002 (2018).
18. L. Sanchis, A. Yanez, P. L. Galindo, J. Pizarro, and J. M. Pastor, Appl. Phys. Lett. **97**, 054103 (2010).
19. A. R. Bekirov, B. S. Luk'yanchuk, and A. A. Fedyanin, JETP Lett. **112**, 341 (2020).
20. O. V. Minin and I. V. Minin, Opt. Quantum Electron. **49**, 54 (2017).
21. I. V. Minin and O. V. Minin, MATEC **155**, 01029 (2018).
22. I. V. Minin and O. V. Minin, *Diffractive Optics and Nanophotonics: Resolution below the Diffraction Limit* (Springer, New York, 2016).
23. W. E. Kock and F. K. Harvey, J. Acoust. Soc. Am. **21**, 471 (1949).
24. W. E. Kock, US Patent No. 2684724A (1948).
25. G. L. Augspurger, Electron. World, 52 (1962).
26. K. Tang, C. Qiu, J. Lu, M. Ke, and Z. Liu, J. Appl. Phys. **117**, 024503 (2015).
27. C. Casagrande and M. Veyssie, C. R. Acad. Sci. (Paris) **306**, 1423 (1988).
28. COMSOL Multiphysics, *Comsol Multiphysics User Guide, Version 4.3a* (COMSOL, AB, 2012), p. 3940.
29. M. Sinha and D. J. Buckley, in *Physical Properties of Polymers Handbook* (Springer, New York, 2007). https://doi.org/10.1007/978-0-387-69002-5_60
30. H. W. Gao, K. I. Mishra, A. Winters, S. Wolin, and D. G. Grier, Rev. Sci. Instrum. **89**, 114901 (2018).

31. M. J. Crocker and J. P. Arenas, Acoust. Phys. **49**, 163 (2003).
32. I. V. Minin and O. V. Minin, Photonics **9**, 762 (2022).
33. J. H. Lopes, M. A. B. Andrade, J. P. Leão-Neto, J. C. Adamowski, I. V. Minin, and G. T. Silva, Phys. Rev. Appl. **8**, 024013 (2017).
34. B. S. Luk'yanchuk, A. Bekirov, Z. Wang, I. V. Minin, O. V. Minin, and A. Fedyanin, Phys. Wave Phenom. **30**, 217 (2022).
35. L. Zhao, T. Horiuchi, and M. Yu, JASA Express Lett. **1**, 114001 (2021).
36. D. Tarrazo-Serrano, C. Rubio, O. V. Minin, A. Uris, and I. V. Minin, Ultrasonics **106**, 106143 (2020).
37. A. D. Pierce, in *Springer Handbook of Acoustics,* Ed. by T. D. Rossing (Springer Science, New York, 2007), Chap. 3, p. 29.
38. O. E. Gulin, Sov. Phys. Acoust. **30**, 276 (1984).
39. C.-Y. Liu, W.-Y. Chen, Y. E. Geints, O. V. Minin, and I. V. Minin, Opt. Lett. **46**, 4292 (2021).
40. Y. Geints, O. V. Minin, and I. V. Minin, J. Opt. **20**, 065606 (2018).
41. E. Lampsijärvi, I. V. Minin, O. V. Minin, J. Makinen, R. Wikstedt, E. Hæggström, and A. Salmi, in *Proceedings of the 2022 IEEE International Ultrasonics Symposium (IUS), October 10–13, Venice, Italy* (2022), p. 1. https://doi.org/10.1109/IUS54386.2022.9957567
42. E. G. Dombrugova and N. N. Chernov, Pis'ma Zh. Tekh. Fiz. **48** (10), 3 (2022).

Translated by R. Tyapaev